JOURNAL OF MATERIALS SCIENCE 13 (1978) 89–96

The flux growth of some new rare earth and iron group complex oxides

B. M. WANKLYN, F. R. WONDRE, B. J. GARRARD, S. H. SMITH
Clarendon Laboratory, University of Oxford, UK

W. DAVISON
School of Physics, University of Newcastle-upon-Tyne, UK

The flux growth of crystals of a number of new rare-earth and transition metal compounds is reported. The following empirical formulae were in good agreement with electron probe microanalysis (EPMA): (Ba, Gd)TiO_3, $R_4Ba_6(BO_3)_9$ (R = Ho to La), $Ni_3Nb_2O_8$, $Ni_8NbB_3O_{15}$, $Ni_2V_2PbO_8$, $Ta_2Co_4O_9$ and $PbCr_{2.3}Ti_{2.3}O_9$. X-ray powder pattern data are given. The growth of crystals of $GdVO_3$, Pb_2CrO_5 and $Ni_3V_2O_8$, which have previously been prepared only as powders, is also reported.

1. Introduction

In exploratory flux growth, it is not unusual to obtain crystals of materials other than those expected, and, since a flux may consist of more than one component, for several compounds to crystallize in a single experiment. This paper describes the growth of a number of new materials, some of which were obtained in this way. Empirical formulae have been derived from EPMA, and X-ray powder pattern data are reported. Many of the materials are expected to exhibit interesting magnetic properties.

2. Chemicals

The following chemicals were used: BDH laboratory reagent grade Na_2CO_3, B_2O_3, BaO, CoO, Cr_2O_3, NiO, PbF_2, PbO, Ta_2O_5, TiO_2, WO_3 and V_2O_5; BDH Optran grade Nb_2O_5; BDH AnalaR grade PbO_2, NaF and Na_2WO_4; Rare Earth Products 99.9% pure R_2O_3; Johnson Matthey V and Ti.

3. Experimental

The furnaces used for crystal growth in air [1] and for growth under reducing conditions [2–4] have been described. For growth in air, the mixed starting materials were contained in platinum crucibles with tightly fitting lids. The crucibles were heated in D-shaped sillimanite muffles to protect the furnaces from attack by corrosive flux vapours [5]. For growth under nitrogen, molybdenum crucibles with molybdenum or graphite lids were used in a nickel-lined vertical tube furnace [3].

The furnaces were heated to the desired initial temperatures at about $100\,K\,h^{-1}$, and after suitable soak periods were slowly cooled in accordance with predetermined programmes. On completion of the slow-cooling programmes, the furnaces were cooled to room temperature at $100\,K\,h^{-1}$. The crystals were separated from the fluxes either by hot draining or by dissolution of the latter in water or dilute nitric acid.

The starting compositions and furnace programmes are given in Table I, together with the crystal products. It should be noted, however, that no attempt has been made to optimize the experimental procedures or growth conditions, except in the case of $GdVO_3$. Details of the preparation and characterization of the various groups of compounds are given in the following sections.

EPMA was used to determine the amount of each of the main constituents (excepting boron) and to detect possible impurities. The resulting data enabled empirical formulae to be calculated. These formulae are, however, provisional until such time as crystal structures are determined. Examination of transparent crystals under the polarizing microscope showed the occurrence of extinction or crystallographic domains.

TABLE I Starting compositions, cooling programmes and crystal products

Formula	Starting composition (amounts in g)	Crucible volume (cm^3)	Initial temp. (° C)	Holding time (h)	Cooling rate ($K\,h^{-1}$)	Final temp. (° C)	Crystal products
$GdVO_3$ $Gd_4Ba_6(BO_3)_9$	57.6 BaO, 16.2 B_2O_3, 13.1 Gd_2O_3, 7.3 V_2O_5, 2.7 V	30	1260	40	2.5	890	Shiny black cubes of $GdVO_3$ up to 1.5 mm × 1.5 mm × 1.5 mm. Transparent colourless rods of $Gd_4Ba_6(BO_3)_9$. Some are shown in Fig. 1a.
$(Ba_{0.93}Gd_{0.07})TiO_3$	57.6 BaO, 16.2 B_2O_3, 13.1 Gd_2O_3, 8 TiO_2, 1.6 Ti	30	1260	5	2	950	Shiny black cubes up to 1 mm × 1 mm × 1 mm
$Nd_4Ba_6(BO_3)_9$	2.7 Nd_2O_3, 11.7 BaO, 3.7 B_2O_3	20	1250	9	2	800	Purple rods 10 mm × 0.5 mm × 0.5 mm
$Pr_4Ba_6(BO_3)_9$	14 Pr_4O_7, 4 Al_2O_3, 54 $BaCO_3$ 9.5 BaF_2, 12 B_2O_3	50	1380	1	1	930	Translucent green prisms up to 6 mm × 4 mm × 3 mm (shown in Fig. 1b).
$Ni_8NbB_3O_{15}$ $Ni_3Nb_2O_8$	8.4 NiO, 7.5 Nb_2O_5, 2.1 B_2O_3, 56 Na_2WO_4, 15.5 WO_3	100	1300	16	3	700	Black hexagonal platelets shown in Fig. 2. Dichroic yellow/green faceted platy crystals. Some are shown in Fig. 3.
$Ni_2V_2PbO_8$	2.4 NiO, 0.6 SiO_2, 41.2 PbO, 18 V_2O_5	100	1290	20	2	900	Black platy rods, orange yellow by transmitted light, up to 2 mm × 1 mm × 1 mm.
$Ni_3V_2O_8$	2.4 NiO, 18 V_2O_5, 41.2 PbO	50	1310	9	2	650	Dark brown hexagonal platelets, golden yellow by transmitted light, shown in Fig. 4.
$Ta_2Co_4O_9$	4.2 CoO, 7.5 Ta_2O_5, 1.7 NaF, 2.1 Na_2CO_3, 7.3 V_2O_5	20	1280	24	1	800	Shiny black prisms up to 2 mm on edge.
$PbCr_{2.3}Ti_{2.3}O_9$	1.5 Cr_2O_3, 0.8 TiO_2 4 PbO, 15 PbF_2	10	1260	5 days			Shiny black needles, 5 to 8 mm long. Some are shown in Fig. 5.
Pb_2CrO_5	9.1 Cr_2O_3, 4.5 NiO, 37 PbF_2, 38 PbO, 1.1 PbO_2	50	1260	27	2	800	Dark red, translucent plates shown in Fig. 6.

4. Notes on the crystals

4.1. $GdVO_3$, (Ba, Gd)TiO_3 and $R_4Ba_6(BO_3)_9$, R = Ho to La

A research programme on the flux growth of compounds containing ions of low valence state included experiments intended to produce crystals of $GdVO_3$ and $GdTiO_3$.

The $BaO-B_2O_3$ flux system, which has previously been used to grow $GdFeO_3$ and other rare earth compounds [6], was used in attempts to produce crystals of $GdVO_3$ and $GdTiO_3$ in molybdenum crucibles under an atmosphere of nitrogen. The flux was melted down in advance and the composition was then adjusted to compensate for the water initially present in the starting materials.

4.1.1. $GdVO_3$

Many trial experiments were performed, of which a few yielded shiny black cubes up to 1.5 mm on edge. EPMA of these crystals showed good agreement with the formula $GdVO_3$, and indicated that little reaction with the crucible had occurred, as shown below:

	Formula requires (wt %)	EPMA of black cubes (wt %)
Gd	61.4	61.2
V	19.9	19.7
Mo	–	0.04

The unit cell dimensions of $GdVO_3$ are similar to those of $GdFeO_3$ and they have similar structures [7, 8]. The X-ray powder pattern of $GdVO_3$, indexed like $GdFeO_3$ [9], is given in Table II. The crystals were rather soft and since they reacted with dilute HNO_3 solution, they were separated from the flux by mechanical methods. The crystals were found to conduct electricity (resistivity ~ 500 ohm cm), like $GdMnO_3$ [10] but unlike $GdFeO_3$, which is an insulator; this property enabled small crystals to be distinguished from the black flux. Magnetic susceptibility measurements indicated a transition at 7.5 K [11] in agreement with published data [12].

TABLE II X-ray powder pattern data for $GdVO_3$

hkl	d_{obs} (Å)	I^*_{estd}	*hkl*	d_{obs} (Å)	I_{estd}
111	3.45	VW	221	1.873	W
020	2.797	VW	131	1.717	S
112	2.708	VS	132	1.602	W
200	2.665	VW	024	1.576	W
021	2.622	VW	312	1.550	VS
022	2.255	VW	Space group: Pb*nm*		
202	2.181	VW			
113	2.116	VW	a = 5.334 Å		
220	1.929	M	b = 5.602 Å		
004	1.904	VW	c = 7.614 Å		

The growth of $GdVO_3$ was adversely affected by the formation of a compound $Gd_4Ba_6(BO_3)_9$, as a result of a reaction with the flux. This compound is described in Section 4.1.3. Similar experiments, which were intended to produce the vanadites of rare earth ions larger than Gd^{3+}, were unsuccessful because of this reaction.

4.1.2. (Ba, Gd)TiO_3

Experiments intended to produce $GdTiO_3$ resulted in small black cubes. EPMA showed that these contained about 5 wt % Gd. The X-ray powder pattern indicated a perovskite structure, with a unit cell slightly smaller than that of $BaTiO_3$ [13], consistent with Gd^{3+} in solid solution in the $BaTiO_3$ lattice and with the empirical formula shown below:

	$(Ba_{0.93}Gd_{0.07})TiO_3$ requires (wt %)	EPMA indicates (wt %)
Gd	4.7	4.5
Ba	54.4	52.6
Ti	20.4	21.0

4.1.3. $R_4Ba_6(BO_3)_9$, (R = Ho to La)

Transparent rods were formed during the experiments described in Sections 4.1.1 and 4.1.2. EPMA showed that the rods obtained from a melt which produced $GdVO_3$ were a product of a reaction between the rare earth oxide and the flux. The empirical formula, $Gd_4Ba_6(BO_3)_9$, is consistent with the EPMA data below:

	$Gd_4Ba_6(BO_3)_9$ requires (wt %)	EPMA indicates (wt %)
Gd	31.7	31.7
Ba	41.6	42.3
V	–	0.4

In subsequent batches, Gd_2O_3 was replaced by other rare earth oxides. It was found that the tendency to form the compounds $R_4Ba_6(BO_3)_9$ increased as the ionic radius of R^{3+} increased. Thus, whereas it was possible to obtain RVO_3 with difficulty in melts with R = Gd, with R = Nd and La only $R_4Ba_6(BO_3)_9$ crystallized.

Batches containing only Pr_4O_7, BaO and B_2O_3, when slowly cooled in air, produced faceted shiny

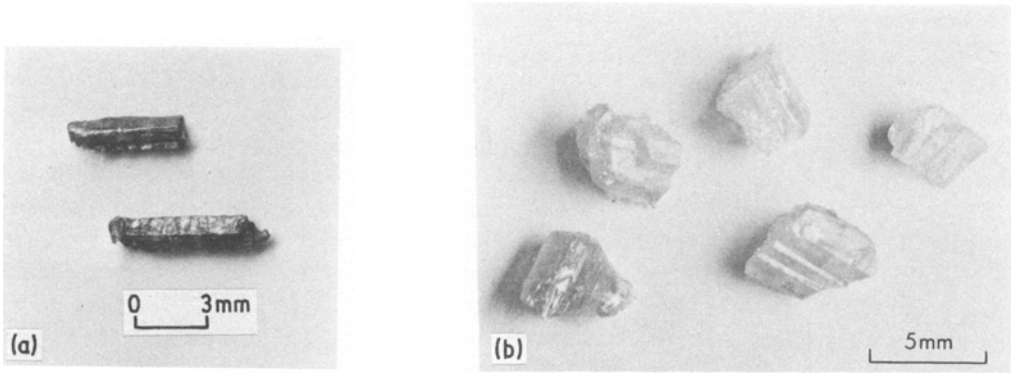

Figure 1 (a) Rods of $Gd_4Ba_6(BO_3)_9$ from $BaO-B_2O_3$ flux. (b) Prisms of $Pr_4Ba_6(BO_3)_9$ from $BaO-BaF_2-B_2O_3$ flux.

rods of $Pr_4Ba_6(BO_3)_9$; the inclusion of BaF_2 in the flux increased the solubility of Pr_4O_7 and yielded larger, thicker prisms. Some are shown in Fig. 1.

Stoichiometric mixtures of the components corresponding to the formula $R_4Ba_6(BO_3)_9$ with R = Ho to La were sintered at 1000° C for 24 h. The X-ray powder patterns of the sinters corresponded closely to those of the crystals. Table III gives X-ray powder pattern data. With rare earth ions smaller than Ho^{3+}, the compound did not form. The crystals were not perfectly smooth, and were etched by water, as occurs with many borates. The crystals were translucent rather than transparent, and their colours were typical of the corresponding rare earth ions. They showed simultaneous extinction.

From the above results, it was evident that $BaO-B_2O_3$ is not suitable for the flux growth of $RTiO_3$ and is by no means ideal for the growth of RVO_3. It should be noted, however, that the oxides of lead and bismuth, which have been components of most fluxes used for the growth of rare earth compounds, are incompatible with Ti^{3+} and V^{3+}, since they are readily reduced by these ions.

TABLE III Diffractometer data for $R_4Ba_6(BO_3)_9$, (R = La, Pr, Nd, Gd, Dy)

I_{est}	R = La d_{obs} (Å)	R = Pr d_{obs} (Å)	R = Nd d_{obs} (Å)	R = Gd d_{obs} (Å)	R = Dy d_{obs} (Å)
VW	4.3	4.2	4.2	4.2	4.2
VW	4.09	4.07	4.07	4.03	4.04
VW	3.99	3.98	3.98	3.94	3.93
VW	3.90	3.90	3.90	3.87	3.87
VW	3.80	3.79	3.79	3.77	3.77
VW	–	–	3.62	3.62	3.62
W	3.53	3.52	3.52	3.52	3.52
W	3.49	3.49	3.48	3.47	3.48
S	3.22	3.20	3.20	3.18	3.18
W	3.19	3.16	3.16	3.13	3.14
MS	3.10	3.08	3.08	3.05	3.05
VS	3.02	3.01	3.01	2.99	2.99
W	2.948	2.937	2.937	2.922	2.929
M	–	2.927	2.927	2.900	2.903
M	2.880	2.857	2.856	2.838	2.840

4.2. $Ni_8NbB_3O_{15}$ and $Ni_3Nb_2O_8$

The starting composition given in Table I yielded four crystalline phases which were identified as $NiNb_2O_6$, $NaNbO_3$ and two new materials, $Ni_8NbB_3O_{15}$ and $Ni_3Nb_2O_8$.

4.2.1. $Ni_8NbB_3O_{15}$

Thin black hexagonal plates, about 1.5 mm × 1.5 mm, were separated from the crystal products. Very thin platelets were green and showed simultaneous extinction. EPMA data were consistent with the formula $Ni_8NbB_3O_{15}$ as shown below:

	Formula requires (wt %)	EPMA indicates (wt %)
Ni	56.3	55.2
Nb	11.1	12.0
W	–	0.2

Some of the plates are shown in Fig. 2. X-ray powder pattern data are given in Table IV.

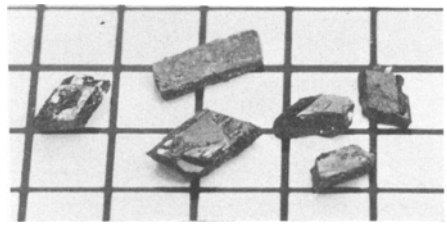

Figure 2 Hexagonal platelets of $Ni_8NbB_3O_{15}$ (mm grid).

TABLE IV X-ray powder pattern data for three new nickel complex oxides

$Ni_8NbB_3O_{15}$		$Ni_3Nb_2O_8$		$Ni_2V_2PbO_8$	
d_{obs} (Å)	I_{est}	d_{obs} (Å)	I_{est}	d_{obs} (Å)	I_{est}
5.84	VW	5.40	VW	6.10	VW
5.30	S	4.46	M	4.94	VW
5.12	VW	3.83	W	4.66	VW
4.89	VW	3.70	W	4.52	VW
3.53	W	3.21	MS	4.33	M
3.04	W	3.14	M	3.76	M
2.915	VW	3.05	S	3.59	W
2.648	VS	2.778	S	3.44	MS
2.611	VW	2.734	S	3.22	VW
2.534	VS	2.663	M	3.07	VW
2.460	M	2.562	S	2.976	VW
2.428	MS	2.517	S	2.840	VS
2.311	M	2.483	MS	2.737	S
2.230	W	2.366	VW	2.496	MS
2.186	W	2.266	VW	2.374	M

4.2.2. $Ni_3Nb_2O_8$

Deep yellow crystals in the form of platy rods were also recovered. They were transparent and dichroic: under the polarizing microscope, they changed from orange-yellow to green instead of showing extinction. EPMA data were in agreement with the formula $Ni_3Nb_2O_8$:

	Formula requires (wt%)	EPMA indicates (wt%)
Ni	35.9	35.1
Nb	37.9	37.7
W	–	3.5

The presence of W^{6+} from the flux in solid solution in the crystals was not unexpected, since the ionic radius is similar to that of Nb^{5+}. Some of the platelets are shown in Fig. 3, and X-ray powder pattern data are given in Table IV.

4.3. $Ni_2V_2PbO_8$

In another experiment, NiO was dissolved in $Pb_2V_2O_7$ flux, the melt was slowly cooled and finally hot-poured at 900° C. Small brittle blackish platy rods were then observed to be attached to the wall and base of the crucible. The rods were poorly formed, orange-yellow by transmitted light, and showed extinction parallel to the longer axis. EPMA data were in agreement with the formula $Ni_2V_2PbO_8$:

	Formula requires (wt%)	EPMA indicates (wt%)
Ni	21.2	20.9
V	18.4	18.7
Pb	37.4	38.9

Stoichiometric amounts of the components corresponding to the formula were sintered at 1100° C for 30 h, ground and resintered at 1000° C for 24 h. The X-ray powder pattern of the sinter corresponded closely to that of the crystals which is given in Table IV.

4.4. $Ni_3V_2O_8$

Another phase was obtained from a similar starting composition to that which yielded $Ni_2V_2PbO_8$, when the melt was allowed to solidify. Some crystals were recovered after the melt had been soaked in warm 1:10 HNO_3 solution for several days. These crystals were dark brown, hexagonal platelets which were yellow by transmitted light and showed simultaneous extinction. Some are shown in Fig. 4. Their X-ray powder pattern was in close agreement with published data for $Ni_3V_2O_8$ [14].

4.5. $Ta_2Co_4O_9$

The crystals were obtained from Na_2O–NaF–V_2O_5 as flux. They were black shiny prisms, 1 to

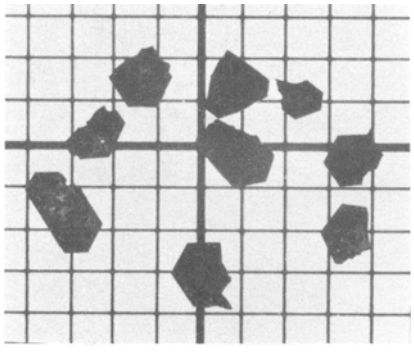

Figure 3 Platy rods of $Ni_3Nb_2O_8$ (2.4 mm grid).

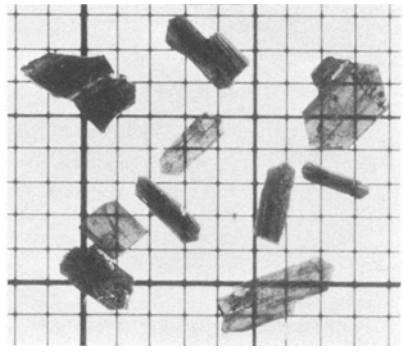

Figure 4 Transparent platelets of $Ni_3V_2O_8$ (mm grid).

2 mm on edge. EPMA data were in good agreement with the formula $Ta_2Co_4O_9$:

	Formula requires (wt %)	EPMA indicates (wt %)
Ta	48.8	48.9
Co	31.8	31.6

The X-ray powder pattern data resembled that of $Nb_2Co_4O_9$ [15] and $Ta_2Fe_4O_9$ [16], and are given in Table V. The structure of $Ta_2Co_4O_9$ is the subject of a current investigation.

TABLE V X-ray powder pattern data for $PbCr_{2.3}Ti_{2.3}O_9$ and $Ta_2Co_4O_9$

$PbCr_{2.3}Ti_{2.3}O_9$		$Ta_2Co_4O_9$	
d_{obs} (Å)	I_{est}	d_{obs} (Å)	I_{est}
7.2	M	4.46	MS
7.1	M	4.20	VW
3.60	W	3.88	W
3.53	W	3.77	W
3.25	M	3.53	VW
3.21	MS	3.34	W
3.16	VS	2.767	VS
3.13	MS	2.581	S
2.928	M	2.356	VW
2.566	W	2.265	W
2.473	VS	2.239	W
2.207	W	2.085	M
2.189	M	1.946	VW
1.888	W	1.890	MS
1.851	M	1.739	S

4.6. $PbCr_{2.3}Ti_{2.3}O_9$

When Cr_2O_3 and TiO_2, in equal molar proportions, were heated with PbF_2, a new crystal material formed as brittle black needles both inside the upper part of the crucible and outside the crucible at its junction with the lid, evidently by either a creeping or a vapour transport process. No similar compound was formed when PbO was substituted for PbF_2. EPMA data indicated that only one phase was present in the needles and an empirical formula $PbCr_{2.3}Ti_{2.3}O_9$ was calculated, which is in good agreement with the analytical data:

	Formula requires (wt %)	EPMA indicates (wt %)
Pb	35.7	36.4
Cr	20.6	20.9
Ti	19.0	18.3
O	24.8	26.2 (fusion analysis)*
F	—	0.2

Sintered samples of the same composition were prepared by holding a stoichiometric mixture overnight at 1250° C. No weight was lost. The X-ray powder pattern of the sinter corresponded closely to that of the crystals. After being heated briefly to the melting point, the quenched melt gave a powder pattern which showed that decomposition had occurred. X-ray powder pattern data are given in Table V, and some of the crystals are shown in Fig. 5.

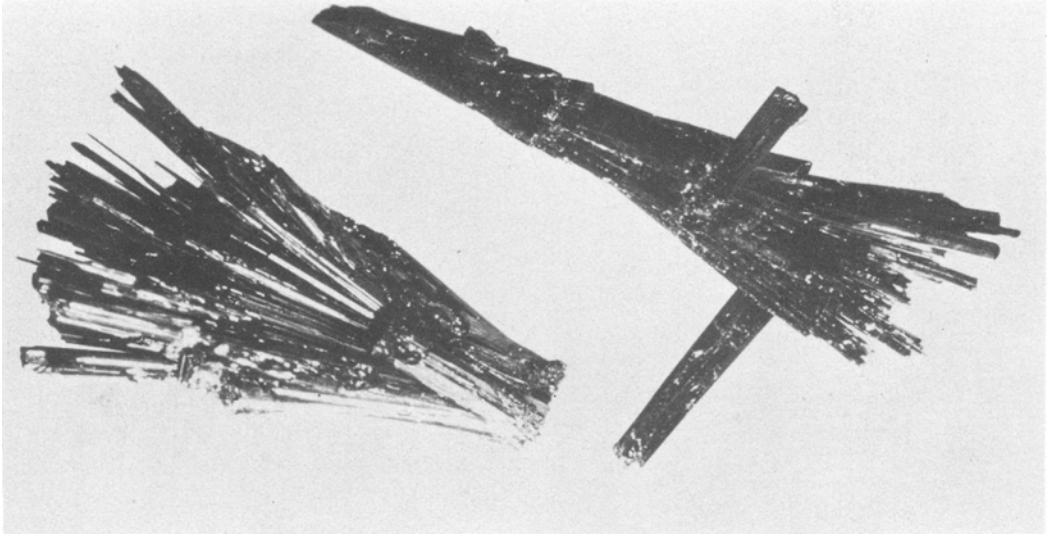

Figure 5 Clumps of black needles of $PbCr_{2.3}Ti_{2.3}O_9$, 6 mm in length.

*Professor O. Knop, Dalhousie University, Nova Scotia, Canada.

4.7. Pb_2CrO_5

When melts containing PbO and Cr_2O_3 in solution are cooled below 1000° C, Cr^{3+} is oxidized to Cr^{6+} and Pb_2CrO_5 crystallizes. This compound melts congruently at 918° C [17]. Starting mixtures of NiO, Cr_2O_3, PbO and PbF_2 were slowly cooled to 800° C in a platinum crucible, which was then inverted to remove the molten material. Brittle dark red translucent plates were observed in the crucible. The crystals showed simultaneous extinction and the X-ray powder pattern agreed with published data for Pb_2CrO_5 [18].

When melts of similar composition were held at 1270° C for 12 days to allow the flux to evaporate, red needles which gave a similar X-ray powder pattern grew on the alumina bricks which blocked the entrance to the muffles. It appears that Cr_2O_3 was transported to the site of crystallization by a vapour species similar to that formed by Al_2O_3 and PbF_2 [19], and that oxidation occurred in the cooler regions of the furnace, followed by deposition of Pb_2CrO_5.

Some of the crystals are shown in Fig. 6. Table VI gives X-ray powder pattern data for the Pb_2CrO_5 crystals grown from the flux, for the vapour-deposited needles, and for the analogous compound Pb_2MoO_5 [20]. Pb_2CrO_5 has been indexed similarly to Pb_2MoO_5; and unit cell dimensions are also given.

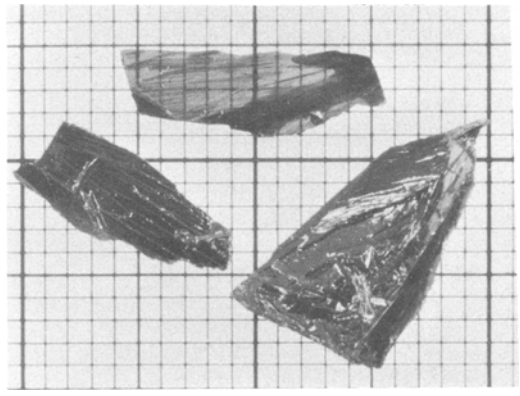

Figure 6 Red plates of Pb_2CrO_5 (mm grid).

Acknowledgements

The authors are grateful to Dr G. Garton for helpful comments and to Mr G. Gwynn for platinum

TABLE VI X-ray powder pattern data for Pb_2CrO_5, indexed as Pb_2MoO_5 [21]

Pb_2MoO_5 [21]			Pb_2CrO_5			
hkl	d_{obs} (Å)	I/I_0	*hkl*	flux grown d_{obs} (Å)	grown by vapour transport d_{obs} (Å)	I_{est}
001	6.71	8	001	6.38	6.54	VW
200	6.51	9	200	6.26	6.35	VW
$20\bar{1}$	6.07	11	$20\bar{1}$	5.93	5.96	VW
$11\bar{1}$	4.53	5	$11\bar{1}$	4.41	4.46	VW
111	3.85	5	111	3.76	3.79	VW
$20\bar{2}$	3.63	5	$20\bar{2}$	3.53	3.59	VW
310	3.47	100	310	3.38	3.42	VS
002	3.35	14	002	3.22	3.29	W
$11\bar{2}$	3.069	80	$11\bar{2}$	2.974	3.033	VS
$40\bar{2}$	3.028	55	$40\bar{2}$		3.000	W
$31\bar{2}$	2.940	45	$31\bar{2}$	2.873	2.908	S
020	2.894	35	020	2.834	2.871	S
202	2.578	17	202	2.505	2.537	M
401	2.550	15	401	2.475	2.510	W
$20\bar{3}$	2.436	5	$20\bar{3}$	2.366	2.409	W
$60\bar{1}$	2.368	12	$60\bar{1}$	2.311	2.347	M
$60\bar{2}$	2.292	25	$60\bar{2}$	2.261	2.277	MS
Monoclinic			Monoclinic			
a_0 = 14.225 Å			a_0 = 13.96 Å		14.10 Å	
b_0 = 5.789 Å			b_0 = 5.661 Å		5.738 Å	
c_0 = 7.336 Å			c_0 = 7.123 Å		7.228 Å	
β = 114.0°			β = 114.6°		114.3°	

work. This work was supported in part by the Science Research Council.

References

1. G. GARTON, S. H. SMITH and B. M. WANKLYN, *J. Crystal Growth* **13/14** (1972) 588.
2. B. J. GARRARD, B. M. WANKLYN and S. H. SMITH, *ibid* **22** (1974) 169.
3. B. J. GARRARD, S. H. SMITH, B. M. WANKLYN and G. GARTON, *ibid* **29** (1975) 301.
4. B. M. WANKLYN, B. J. GARRARD and G. GARTON, *ibid* **33** (1976) 150.
5. B. M. WANKLYN and Z. HAUPTMAN, *J. Mater. Sci.* **9** (1974) 1078.
6. R. C. LINARES, *J. Amer. Ceram. Soc.* **45** (1962) 307.
7. S. GELLER, *Acta Cryst.* **10** (1957) 243.
8. F. BERTAUT and F. FORRAT, *J. de Phys. et Rad.* **17** (1956) 129.
9. S. GELLER and E. A. WOOD, *Acta Cryst.* **9** (1956) 563.
10. B. M. WANKLYN, *J. Mater. Sci.* **7** (1972) 813.
11. A. H. COOKE and M. R. WELLS, Private communication.
12. R. BOZORTH, H. J. WILLIAMS and D. E. WALSH, *Phys. Rev.* **103** (1956) 572.
13. ASTM 8-372.
14. ASTM 22-1194.
15. ASTM 13-464.
16. ASTM 19-633.
17. F. M. JAEGER and H. C. GERMS, *Z. Anorg. u allgem. Chem.* **119** (1921) 155.
18. ASTM 21-946.
19. B. M. WANKLYN and G. GARTON, *J. Mater. Sci.* **9** (1974) 1378.
20. ASTM 24-579.

Received 16 March and accepted 28 April 1977.